Journal of Surface Investigation

COUNTRY	SUBJECT AREA AND CATEGORY	PUBLISHER	H-INDEX
United States Universities and research institutions in United States Media Ranking in United States	Materials Science Nanoscience and Nanotechnology Surfaces, Coatings and Films	Pleiades Publishing	25

PUBLICATION TYPE	ISSN	COVERAGE	INFORMATION
Journals	10274510, 18197094	1997-2001, 2007-2023	Homepage How to publish in this journal

SCOPE

Journal of Surface Investigation: X-ray, Synchrotron and Neutron Techniques publishes original articles on the topical problems of solid-state physics, materials science, experimental techniques, condensed media, nanostructures, surfaces of thin films, and phase boundaries: geometric and energetical structures of surfaces, the methods of computer simulations; physical and chemical properties and their changes upon radiation and other treatments; the methods of studies of films and surface layers of crystals (XRD, XPS, synchrotron radiation, neutron and electron diffraction, electron microscopic, scanning tunneling microscopic, atomic force microscopic studies, and other methods that provide data on the surfaces and thin films). Articles related to the methods and technics of structure studies are the focus of the journal. The journal accepts manuscripts of regular articles and reviews in English or Russian language from authors of all countries. All manuscripts are peer-reviewed.

Join the conversation about this journal

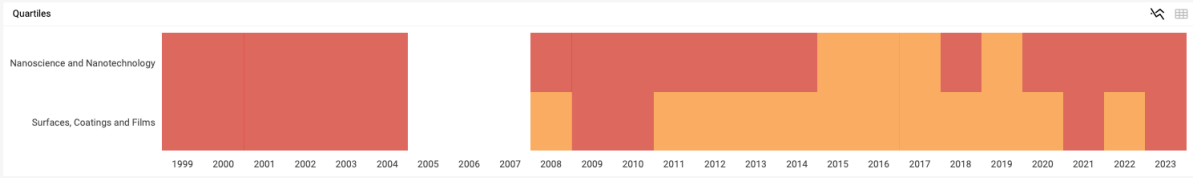

ISSN 1027-4510, Journal of Surface Investigation: X-ray, Synchrotron and Neutron Techniques, 2024, Vol. 18, No. 2, pp. 495–505. © Pleiades Publishing, Ltd., 2024.

Microstructure and Mechanical Properties of Laser Clad18Ni300 Coatings with La_2O_3 Addition on ZL205A Aluminum Alloy

Qixiao Xu[a, b], Daoyou Zheng[c], Xiao Chen[d], Sergey Konovalov[e], and Xizhang Chen[b, *]

[a] *China University of Petroleum (East China), Qingdao, 266400 China*

[b] *Zhejiang Industry and Trady Vocational College, Wenzhou, 325300 China*

[c] *Wenzhou University, Wenzhou, 325000 China*

[d] *Laiwu Branch of Shandong Iron and Steel Co., Ltd., Shandong, China*

[e] *Siberian State Industrial University, Novokuznetsk, 6564007 Russia*

*****e-mail: chenxizhang@wzu.edu.cn*

Received August 22, 2023; revised October 10, 2023; accepted October 10, 2023

Abstract—The preparation of Fe-based wear-resistant coating by high-speed laser cladding method can well solve the problem of poor wear resistance of aluminum alloy surface. However, due to the large expansion coefficient difference of Fe and Al, the Fe-based laser cladding layer on the Al surface often has cracks, poor molding morphology, and poor mechanical properties. In this work, La_2O_3 is added as an additive in order to improve the morphology and mechanical properties of Fe-based laser cladding layer on the surface of Al alloy. High-speed laser cladding technology was used to prepare the coating of 18Ni300 + XLa_2O_3(X = 0.5, 1, 1.5, 2 wt %) on ZL205A aluminum alloy. The morphology, microstructure, hardness, wear resistance and heat shock resistance of the cladding layer were studied. The morphology and crack characteristics of the fusion zone were observed by scanning electron microscopy. Under the present test conditions, the addition of La_2O_3 improved the forming morphology, refined the microstructure of the cladding, and significantly improved the mechanical properties of the cladding. The optimal addition of La_2O_3 with the best properties was 1.5 wt % which provided: flat cladding surface, absence of internal cracks, refined grain size, improved wear resistance and thermal shock resistance, 47% higher hardness when compared to 18Ni300.

Keywords: Laser cladding, Rare earth oxide, Wear-resistant coating

DOI: 10.1134/S102745102402037X

1. INTRODUCTION

In automotive engines, the volume and mass of the engine account for a large proportion of the whole vehicle. As the automotive industry moves towards light-weighting, using lighter metals instead of cast iron for engines has become a popular choice by car manufacturers [1]. ZL205A (Al–Cu based alloy) is the world's strongest cast aluminum alloy, and has high toughness, which can meet the mechanical performance requirements of various large and high-speed new aviation aircraft, and is widely used in aerospace and auto parts production [2].

At present, the vast majority of engines are piston engines. In piston engines, the inner surface of the engine cylinder and the piston undergo long-term high-speed friction; withstand complex alternating loads, but also experience thermal shock due to cylinder gas combustion and cooling Hence, piston engine cylinder needs higher requirements for abrasion resistance and heat shock resistance of cylinder inner surface. However, the low hardness and wear resistance of aluminum alloy hinder its application in engine production. The traditional way to solve this problem is to embed the inner lining of the aluminum alloy cylinder, which can solve the problem of poor wear resistance of the inner wall of the aluminum alloy engine cylinder to a certain extent. However, due to the difference of expansion coefficient between cylinder block and cylinder casing, it is difficult to withstand long-term thermal shock.

Laser surface cladding technology which involves the incorporation of a cladding layer on the metal substrate that provide better in terms of hardness, wear resistance and corrosion resistance than the substrate [3–5]. Compared with other surface reinforcement methods, wear-resistant coating prepared by laser coating combined with matrix metallurgy has the advantages of flexibility, high controllability, cleanliness and no pollution, and is widely used in surface reinforcement, additive manufacturing and product maintenance [6].

However, there are still series of difficulties in the preparation of laser cladding wear-resistant layer on the surface of aluminum alloys such as generation of large residual stress inside the cladding layer and formation of cracks on the cladded layer due to excessive residual stress. Further, as the laser cladding process is a rapid non-equilibrium process consisting of extreme cold and extreme heat, the clad layer gets easily mixed with impurities, which forms brittle phases [7–9], thereby reducing the overall toughness of the cladding layer. These two aspects, in combination, result in cracking of the cladded layer on the aluminium alloy surface, such that the performance of the cladding layer becomes ineffective.

Rare earth elements and their oxides can play a role in enhancing toughening because of their special physical and chemical properties, and are often used as laser cladding additives [10]. Due to the large atomic radius of rare earth elements, they are easy to enrich at grain boundaries and defects, which will play a role in purifying grain boundaries, inhibiting component overcooling, preventing chemical component segregation, and refining grains [11]. The chemical properties of rare earth elements are relatively active, and they are easy to react with O, S and other impurity elements in the laser melting pool, forming stable compounds and floating in the molten pool, thus playing a role in purifying tissues [12]. In addition, rare earth oxides also have the effect of promoting convection in the molten pool. The use of even small amount of rare earth oxides as additives can improve the structure and performance of the cladding layer by reducing the defects and resist cracks.

The method of adding rare earth oxides can also be applied to laser cladding of aluminum alloy. Liang J [7] used laser cladding technology to prepare Ni60 alloy cladding layer on 6063Al surface with 4%CeO_2, 5%Y_2O_3 and 5%La_2O_3. The distribution of elements, the nucleation and growth mechanism of interfacial transition layer and upper cladding layer, and the action mechanism of rare earth elements were analyzed from the perspectives of thermodynamics and dynamics. Zhang [13] prepared 2% (mass fraction) CeO_2/Ni60A cladding layer on 6063 aluminum alloy by laser cladding technology. The microstructure, microhardness and corrosion resistance of the coating were studied. The results show that compared with Ni60A cladding layer, 2% CeO_2/Ni60A cladding layer has more uniform microstructure, smaller grain size and smaller porosity. Xie [14] used the optimized process parameters to laser cladding the alloy powder Ni60+ rare earth Y_2O_3 on the surface of 6063 aluminum alloy, and studied the influence of different rare earth contents on the strengthening layer to obtain the best rare earth content. Wang [15] used laser cladding technology on 6063 aluminum alloy surface Ni60, Ni60 + 4%CeO_2, Ni60 + 5%Y_2O_3 and Ni60 + 5%La_2O_3 laser cladding treatment, and then carried out hardness and high temperature friction and wear experiments, by analyzing the friction coefficient of each sample, wear mark profile, wear amount, phase, composition and after wear. The wear resistance and wear mechanism of each sample were analyzed, as well as the influence of rare earth on the wear resistance and wear mechanism of the cladding layer. By laser cladding technology. Fu [16] prepared Ni60 alloy cladding layers with rare earths (5%La_2O_3, 5%CeO_2 and 5%Y_2O_3) on 6061Al surface, respectively. The thickness of the cladding layers containing three rare earths reached 1000 μm, without obvious pores and cracks, and had good cross-section morphology. The proper amount of rare earth can improve the fluidity of molten pool, reduce or eliminate the porosity and crack defects of cladding layer, and improve the corrosion resistance of cladding layer. In the researches of domestic and foreign researchers in this field, aluminum alloys used for laser cladding matrix are mostly common aluminum alloys such as 6063 and 5083. ZL205A is an important aluminum alloy material in the field of aviation and aerospace, and the researches in this field are relatively scarce. On the other hand, the basic materials of cladding layer are mostly concentrated in Ni-base alloy powder and Al-base mixed powder, and there is a lack of relevant research on Fe-base alloy powder.

In this study, the effect of La_2O_3 addition on the morphology and mechanical properties of Fe-based laser cladding layer on ZL205A aluminum alloy surface was investigated. Using high-speed laser cladding technology, 18Ni300 + XLa_2O_3 (x = 0.5, 1.0, 1.5, 2.0 wt %) coated layers were prepared on ZL205A aluminum alloy surface, and the molding morphology, microstructure, mechanical properties and thermal shock resistance of the five cladding layers were compared and analyzed.

2. MATERIALS AND METHODS

2.1. Materials

The base material is cast ZL205A aluminum alloy (specified according to GB/t1173-1995), and its chemical composition is shown in Table 1. 18Ni300 alloy powder was used as the raw material for laser cladding, and the chemical composition was shown in Table 2. Lanthanum oxide (La_2O_3) powder was added to the 18Ni300 base cladding materials in 0.5, 1, 1.5, 2 wt % and the blends were mixed in a ball mill to get desired (18Ni300 + X wt % La_2O_3) composite powder.

Table 1. Nominal chemical composition of ZL205A aluminum alloy in wt %

Cu	Mn	Ti	Cd	V	Zr	B	Al
4.6–5.3	0.3–0.5	0.15–0.35	0.15–0.25	0.05–0.3	0.05–0.2	0.005–0.06	Rest

Table 2. Chemical composition of 18Ni300 powder in wt %

Ni	Mo	Co	Ti	P	Mn	C	Fe
18–19	4.6–5.2	8.5–9.5	0.5–0.8	≤0.01	≤0.1	≤0.03	Rest

a. Laser processing parameters. Central powder feeding high-speed laser cladding equipment (ZkZM-6000, Zhongke Zhongmei Laser Technology) was used for high-speed laser cladding on ZL205A plate. Figure 1 shows the schematic diagram of laser spraying of central powder. Compared with conventional laser cladding, the laser energy in the process of fast laser cladding is mainly on the cladding powder, and the heat input to the matrix is small, so the high speed laser cladding is especially suitable for aluminum alloy surface strengthening [17]. The laser cladding process parameters are shown in Table 3.

b. Morphological and microstructural characterization. The surface of the cladded layer was analyzed for degree of flatness, presence of defects, line warpage, cracks on surface or at the root, and cladded layer-cladded layer distortion. The thickness of the coating was measured by a micro coating range finder and the surface defects were determined by dye penetrant test. Microstructure of the cross section of cladding layer was observed by SEM. Coated samples were cut, ground and mechanically polished, and then etched in an etching agent consisting of HNO_3 and HF with a volume ratio of 2 : 1. The elements content quantification was conducted by energy dispersive spectroscopy (EDS).

c. Mechanical testing. Microhardness measurements were carried out (normal to surface up to the substrate at 0.1 mm equidistant points) on the metallographic specimen by HV-1000A microhardness tester. The friction and wear test of cladded layer was carried out in a MFT-EC4000 reciprocating sliding wear tester. Friction values and weight loss of the sample before and after the test was calculated, and the worn samples were observed and analyzed by SEM.

Heat-shock resistance test of the cladding layer is conducted using a box-type resistance furnace. It involves keeping the sample warm in a 520°C resistance furnace for 10 min and then cooling it in water at room temperature. Thermal shock resistance was assessed by recording the number of heating-cooling times until the cladding layer failed. The quenched samples were visually inspected and the visually observable macro-cracks on the surface and at the interface were observed with a magnifying glass of 10x magnification. The criteria for failure under thermal shock (defined as the crack initiation life under thermal shock) were considered as the number of thermal shocks for which the macroscopic cracks appear for the first time, and peeling of the cladded layer or the occurrence of cracks in more than 1/3 of the area.

3. RESULTS AND DISCUSSION

3.1. Morphology of the Cladded Layer

It can be seen from Fig. 2, that although the cladded layers deposited with 18Ni300 has a rough and corrugated morphology, it is mostly free from surface defects except larger circular crack dispersed near the edges. The alloy particles that are not melted on the surface can be worn off to reveal a smooth metallic appearance, but deep pits remain on the surface. This can be attributed to a very short action time of laser over the molten pool causing low fluidity of molten pool, which resulted in solidification of unmelted particles before they can be discharged from the molten pool.

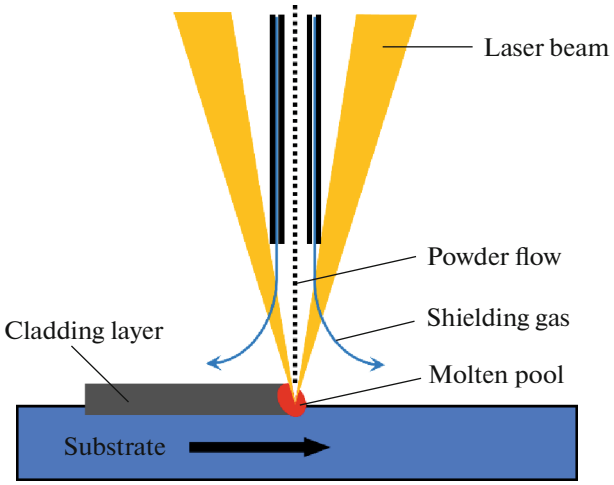

Fig. 1. Schematic of central powder feeding laser cladding.

Table 3. Laser cladding process parameters

Laser cladding process parameters	Values
Laser power, kW	1.5
Laser scanning speed, mm/s	20
Powder feed rate, g/min	15
Lap rate, %	30
Spot diameter, mm	0.5

The macro-morphology of the 18Ni300 + X wt % La_2O_3 (X = 0.5, 1, 1.5, 2%) laser cladded layer is shown in Fig. 3. Addition of La_2O_3 resulted in improvement of the corrugated morphology and the cladded layer gradually became flat with the increase of La_2O_3 content. This is because the rare earth oxide La_2O_3 enhances fluidity of liquid metal and the laser absorption rate of the powder. The dye penetrant tests results of the 18Ni300 + X wt % La_2O_3 cladding as shown in Figure 4 suggest that with the addition of La_2O_3, the number of pits on the cladded layer surface is reduced. When the additive amount is for 1.5 wt % La_2O_3, no obvious pits can be observed on the cladded layer surface. However, when the amount of La_2O_3 is further increased to 2% by weight, the surface of the cladding layer cracks greatly, and it is difficult to form a good metallurgical bond with the matrix. A large number of unmelted rare earth oxide particles will destroy the continuity of the cladding layer, affect the normal formation of the cladding layer, and eventually cause problems such as poor bonding and cracking with the substrate (see Fig. 3e). Because 18Ni300 + X wt % La_2O_3 did not form metallurgical bond with the matrix and the surface cracking was serious, no penetration detection was conducted on this sample.

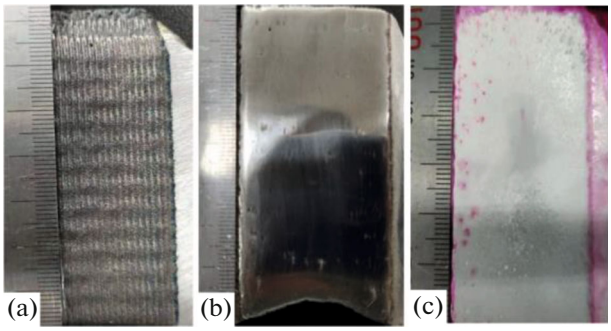

Fig. 2. Macro-morphology of 18Ni300 cladded layer: (a) initial morphology; (b) after grinding; (c) after Dye penetrant tests.

3.2. Microstructure Analysis

Figures 5(a1) and 5(a2) shows the comparison of the overall microstructure between the 18Ni300 and 18Ni300 + 1.5 wt % La_2O_3 cladded layers. It denotes that compared with the cladding without additives, the cladding with rare earth oxide has no pitting pores and slag inclusions on the surface, and the microstructure of cladding is more uniform. Surface-active rare earth elements promote the purification of the cladding layer, improve the overall morphology of the grains in the fusion zone of the cladding, and make the fusion line more even and flat. Figures 5(b1) and 5(b2) compared the microstructure of fusion zones of 18Ni300 and 18Ni300 + 1.5 wt % La_2O_3 claddings. The microstructure of the fusion zone of 18Ni300 cladding without additives is more chaotic inhomogeneous. There are no large inclusions and microcracks in the fusion zone of 18Ni300 + 1.5 wt % La_2O_3. The grains in the fusion zone of 18Ni300 + 1.5 wt % La_2O_3 cladded layer are finer. This is because rare earth oxides improve the fluidity of melt, strengthen the convection of the pool

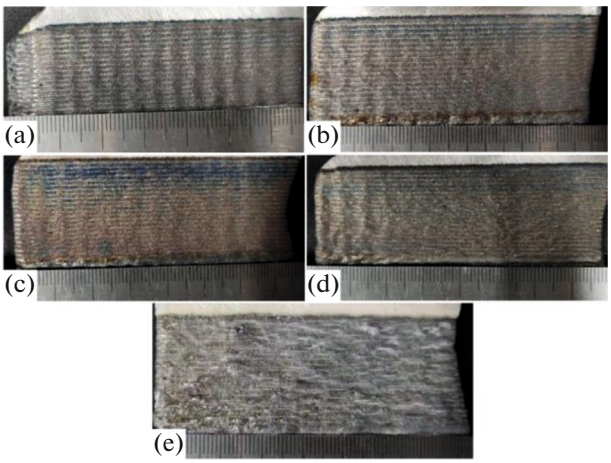

Fig. 3. Macro-morphology of 18Ni300 + X wt % La_2O_3 laser cladded layer: (a) X = 0; (b) X = 1 wt %; (c) X = 1.5 wt %; (d) X = 2 wt %.

and disrupt the growth of columnar crystals. In addition, the existence of rare-earth atoms with large atomic radius in the solid solution will cause a lot of lattice distortion and increase the total energy of the system. Therefore, rare-earth elements are more inclined to be enriched at the grain boundary to maintain the lowest free energy of the system. Rare-earth atoms enriched at the grain boundary hinder the growth process of grains, thus refining the microstructure of the cladding layer [18]. Figure 5(c1) and 5(c2) shows the microstructure of the core region of the 18Ni300 and 18Ni300 + 1.5 wt % La_2O_3 claddings. The grains of cladding with La_2O_3 addition are finer and do not show directionality. In Fig. 5 (c1), the average grain size of 18Ni300 is 38.288um2. In Fig. 5(c2), the average grain area of 18Ni300 + 1.5 wt % La_2O_3 is 9.309um2, which is 24.3% of 18Ni300. Figures 5(d1) and 5(d2) exhibits shows the comparison of microstructure of the top region of 18Ni300 and 18Ni300 + 1.5 wt % La_2O_3 cladded layers. The microstructure of the cladding without La_2O_3 possesses large number of impurities and pores, and the grain morphology is inhomogeneous; whereas the cladding with La_2O_3 additions has significantly lower impurities, and the microstructure is more uniform and finer.

As shown in Fig. 6, the SEM images show heterogeneous phases in the bonded zone of 18Ni300 cladded layer, which are the heterogeneous phases present in the bonded zone of 18Ni300 cladded layer are non-continuously distributed in blocks near the interface. EDS point analysis results of this block (Table 4) show that the inclusions at point 1 are composed of Al and O with a concentration ratio of 3 : 2, which is determined to be Al_2O_3.The Al_2O_3 is lighter and solidifies above the fusion line. The major constituent at points 2, 3 and 4 are found to be Fe and Al. According to elemental analysis, it can be inferred that these blocks are $FeAl_3$, Fe–Al and Fe_2Al_5 respectively. Figure 6 also indicates presence of microcracks in the bonded zone of 18Ni300 cladded layer, which occurs near the serration at the bottom of the cladded layer. The cracks apparently cut across the serration, but do not spread over large area. As can be seen from Fig. 6, the zigzag morphology of the bonding zone of 18Ni300 + 1.5 wt % La_2O_3 cladding layer is obviously improved, and a good metallurgical bonding is formed between the cladding layer and the substrate, without cracking. EDS analysis showed that Fe–Al intermetallic compounds still existed in the binding zone of 18Ni300 + 1.5 wt % La_2O_3 cladding layer. It can be seen that the addition of La_2O_3 cannot inhibit the formation of intermetallic compounds, but can inhibit the formation of Al_2O_3. This is because rare earth elements are chemically active and preferently form oxides with oxygen elements. In addition, the addition of La_2O_3 can effectively promote the flow of the molten pool, make the transition of the fusion zone smoother, and accelerate the discharge of impurity elements, so as to play a role in purifying the tissue.

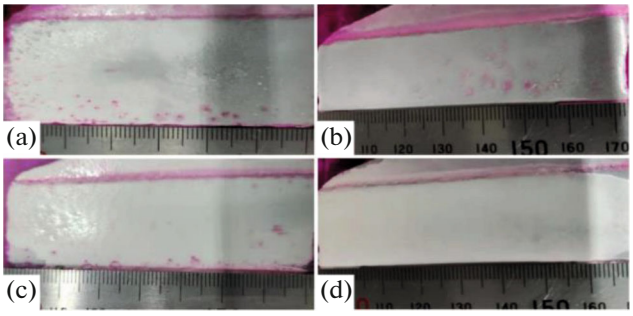

Fig. 4. Macro-morphology of the laser cladded layer after Dye penetrant tests: (a) 18Ni300; (b) 18Ni300 + 0.5 wt % La_2O_3; (c) 18Ni300 + 1 wt % La_2O_3; (d) 18Ni300 + 1.5 wt % La_2O_3.

3.3. Hardness of the Cladded Layer

Figures 8a and 8b the distribution and average hardness of 18Ni300 + X wt % La_2O_3 cladding. It can be seen that the Addition of La_2O_3 improves the microhardness. When the content of rare earth oxide is 1.5 wt %, the hardness of the cladding is 1.37 times that without additives. Due to the addition of rare earth oxide, the microhardness of the cladding was improved by The observed increase is due to the dual effects of grain refinement and solid solution strengthening. Furthermore, after adding rare earth oxide, the hardness values of the cladding is stable changes gradually and stably, which is related to the purifying effect on microstructure that promoted the flow of molten pool. However, when the rare earth oxide is added excessively (2 wt %), the microstructure of the clad-

Table 4. EDS point analysis results

Elements	C	O	Al	Fe	Ni	Mo
Point 1	0	55.6	34.8	8.5	0.9	0.2
Point 2	18.4	13.7	13.5	42.4	11.3	0.7
Point 3	14.3	5.3	34	36.3	9.4	0.7
Point 4	14.8	15.5	43.2	21.5	4.5	0.5
Point 5	14.3	1.4	34	36.3	9.4	0.7
Point 6	14.8	2.1	43.2	21.5	4.5	0.5

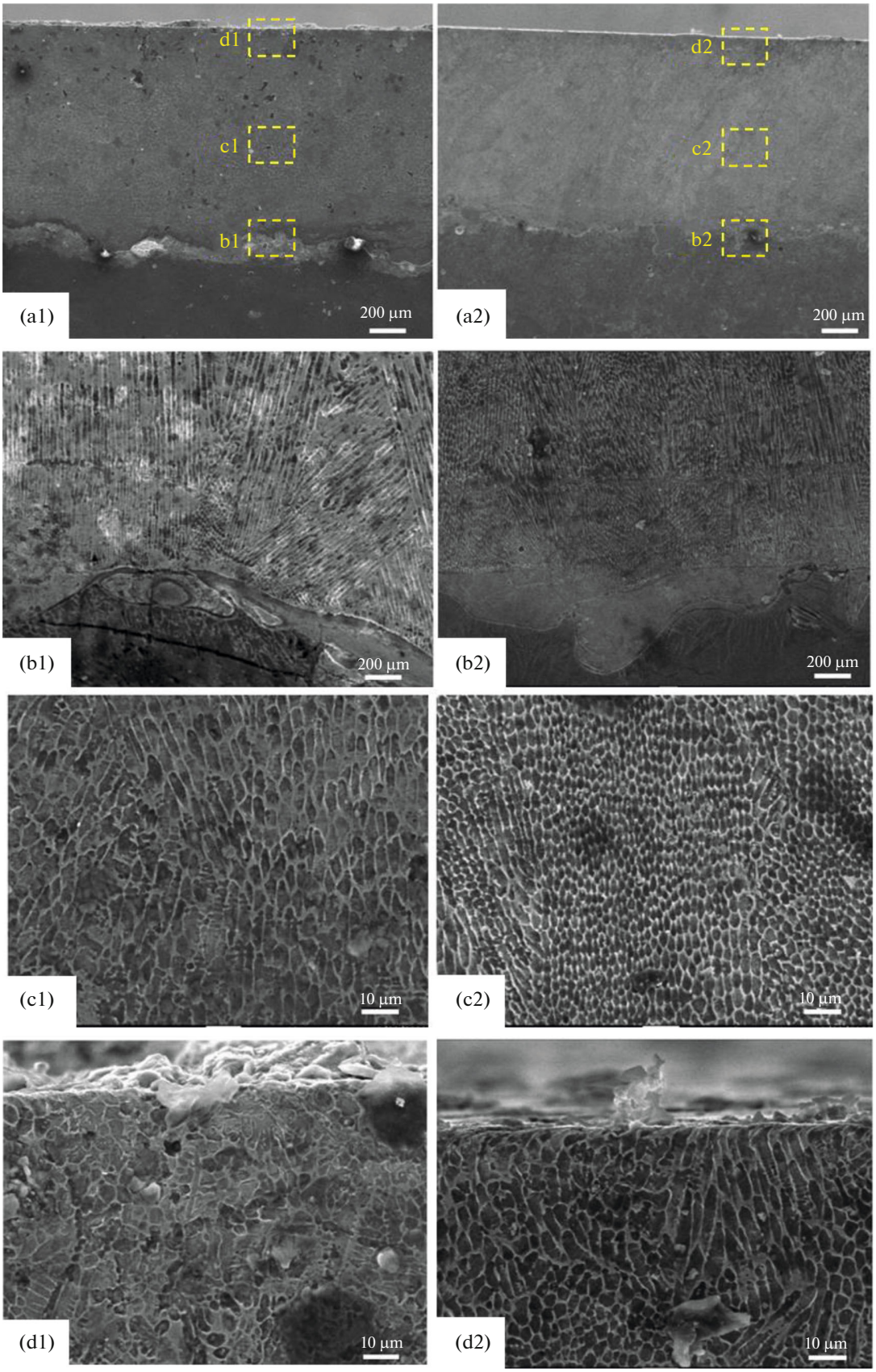

Fig. 5. Comparison of microstructure in the 18Ni300 and 18Ni300 + 1.5 wt % La_2O_3 cladded layers: (a1), (b1), (c1), (d1) 18Ni300; (a2), (b2), (c2), (d2) 18Ni300 + 1.5 wt % La_2O_3.

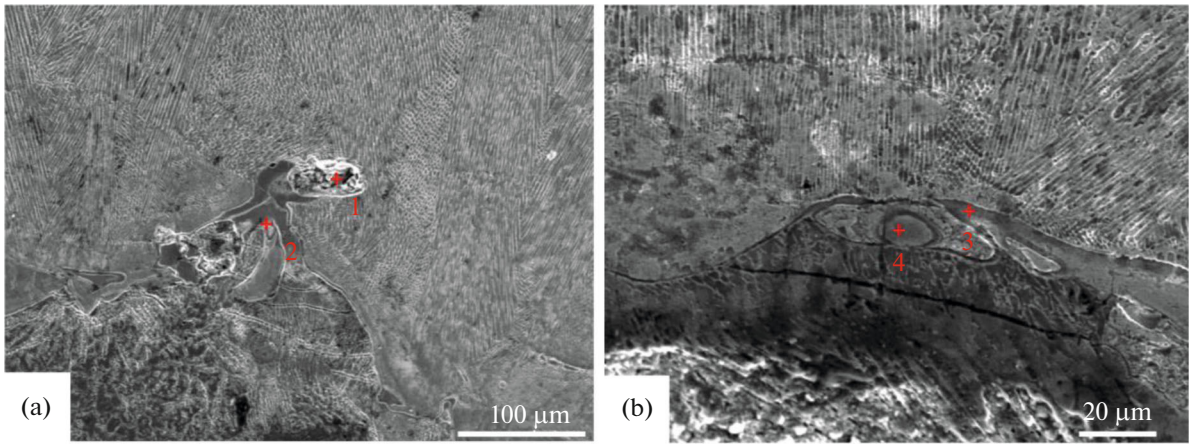

Fig. 6. Heterogeneous phases and micro-cracks in bonded zone of 18Ni300 cladded layer.

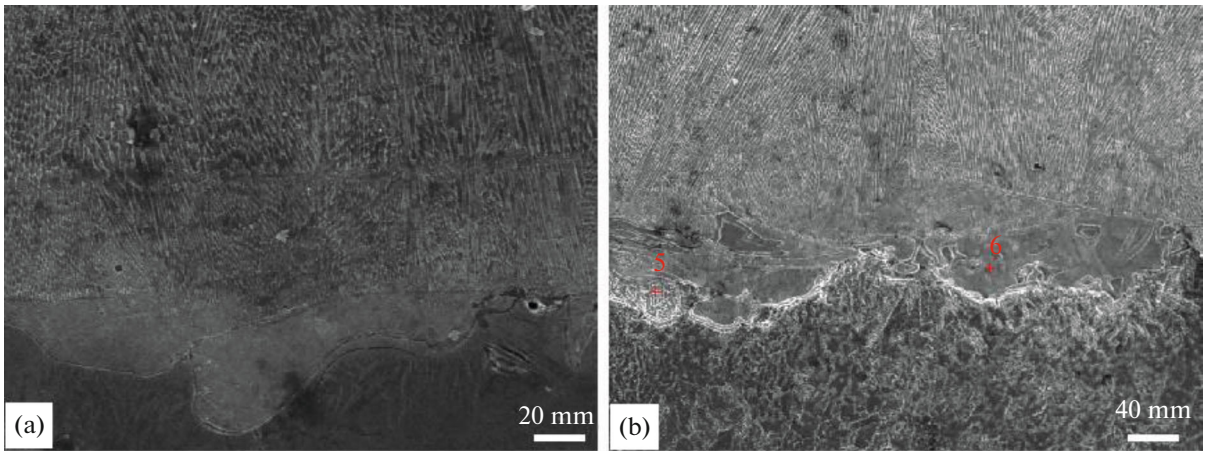

Fig. 7. Heterogeneous phases in bonded zone of 18Ni300 + 1.5 wt % La_2O_3 cladded layer.

ding becomes more inhomogeneous and thus the hardness values also vary changes dramatically.

3.4. Wear Resistance of the Cladded Layer

The results of wear test of 18Ni300 + X wt % La_2O_3 are shown in Fig. 9. It can be seen that (18Ni300 + 1.0 wt % La_2O_3) and (18Ni300 + 1.5 wt % La_2O_3) cladding have shown smaller friction loss and similar equal wear resistance. Compared with the cladding without additives, the wear resistance of the layer cladded with 1.5 wt % La_2O_3 is increased by 1.4 times. The friction coefficient curves of 18Ni300 and 18Ni300 + 1.5 wt % La_2O_3 cladded layer are shown in Fig. 10. Compared with the cladded layer without additives, the friction coefficient of the cladded layer with 1.5 wt % La_2O_3 addition is significantly reduced, indicating that the wear reduction of the cladded layer is reduced after adding La_2O_3.

The morphology of worn surface of 18Ni300 + X wt % La_2O_3 cladding is shown in Fig. 11. It can be seen that the increase of La_2O_3 leads to the reduction of the number of wear marks and the shallower depth

Table 5. EDS analysis results of wear zone composition of 18Ni300 and 18Ni300 + 1.5 wt % La_2O_3

Elements	C	O	Cr	Fe	Co	Ni	Cu	Mo
Point 1	3.8	38.83	4.8	44.19	1.15	2.34	0.68	0.48
Point 2	3.6	4.7	7.36	56.5	9.12	10.89	0.53	2.7
Point 3	3.48	17.21	0.28	55.84	5.88	14.14	0.66	2.51
Point 4	7.35	2.03	5.66	66.57	5.11	10.93	0.45	1.90

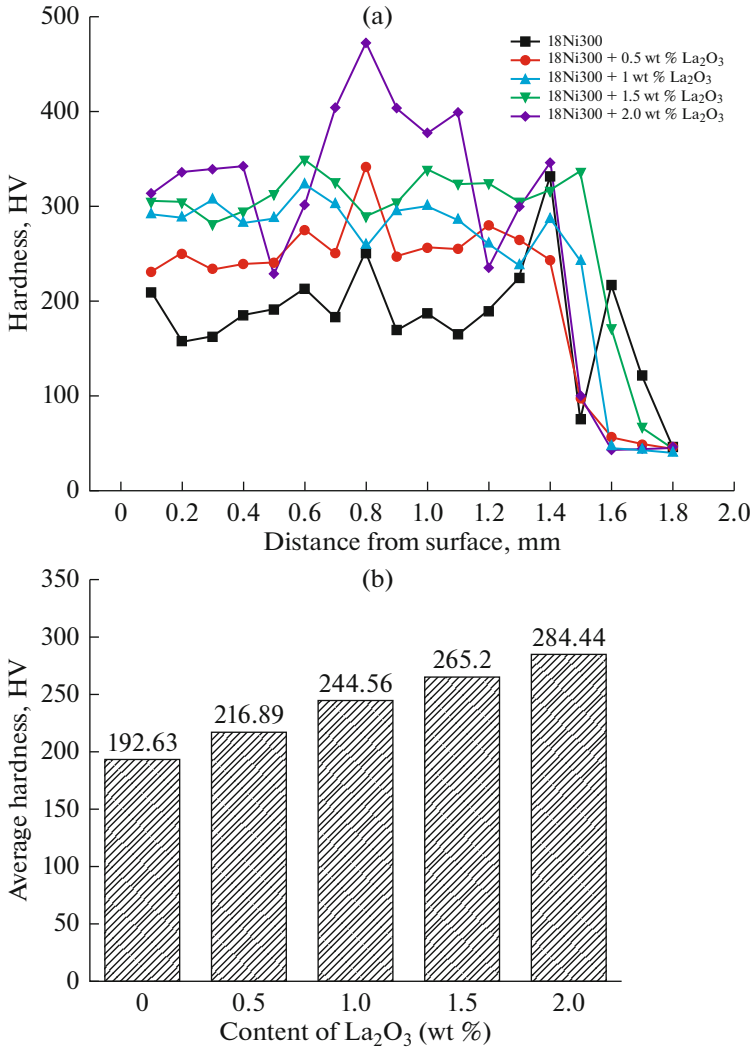

Fig. 8. Hardness distribution (a) and (b) average hardness of 18Ni300 + X wt % La_2O_3 laser cladded layer.

of wear marks. Small scale spalling pits were observed for the cladding with higher content of La_2O_3, which indicates that the main wear form of the cladding is adhesive wear. Figure 12 depicts comparison of 18Ni300 and 18Ni300 + 1.5 wt % La_2O_3 cladded layers at a higher magnification. EDS point scanning was performed to identify elemental composition. The results of EDS analysis are shown in Table 5. It can be observed that the oxygen content on the worn surface of cladded layers with rare earth oxide is reduced, which indicates that rare earth oxide can inhibit oxidation wear. This is because La_2O_3 refined the particles in the cladding layer, so that the texture becomes dense and uniform, and the hardness of the cladding layer can be improved. This also conforms to the rule that material hardness is inversely proportional to wear loss, that is, the greater the hardness, the smaller the wear loss. On the other hand, rare earth can improve the resistance of material surface to contact fatigue damage under lubrication condition [19, 20], which further improves the wear resistance of cladding surface. When the content of La_2O_3 is 2.0%, the excess rare earth and the impurity elements in the powder produce refractory compounds, which makes the coating microstructure become larger and the surface quality deteriorates, thus reducing the wear resistance of the cladding layer.

3.5. Thermal Shock Resistance of the Cladded Layer

Figure 13 shows the thermal shock times of cracking and failure of 18Ni300 + X wt % La_2O_3 cladded layer. It can be seen that when La_2O_3 is used, as additive, the thermal shock resistance of the cladded layer is improved, and the thermal shock resistance of the cladded layer is improved by 41% when the addition

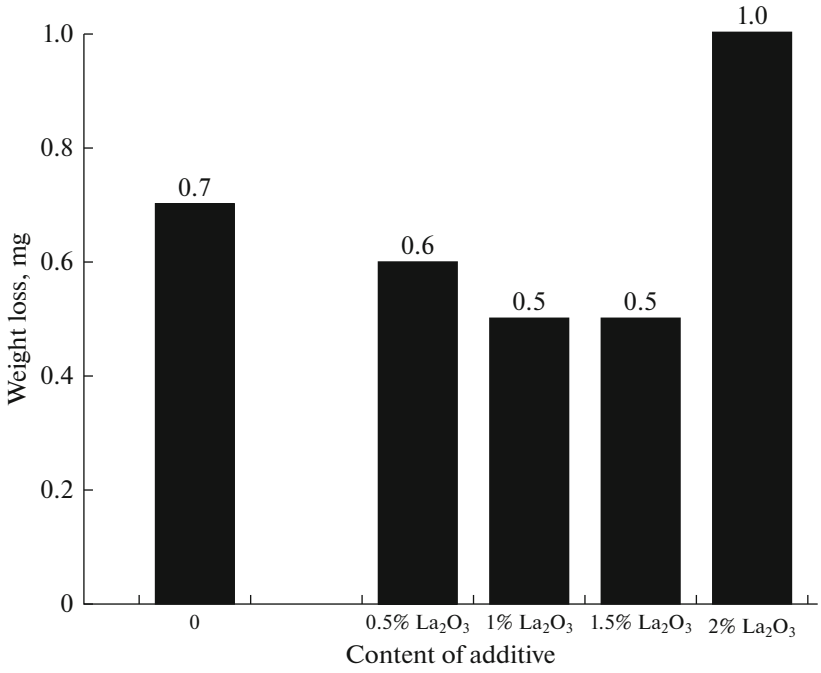

Fig. 9. Weight loss test results of 18Ni300 coatings with different proportions of additives.

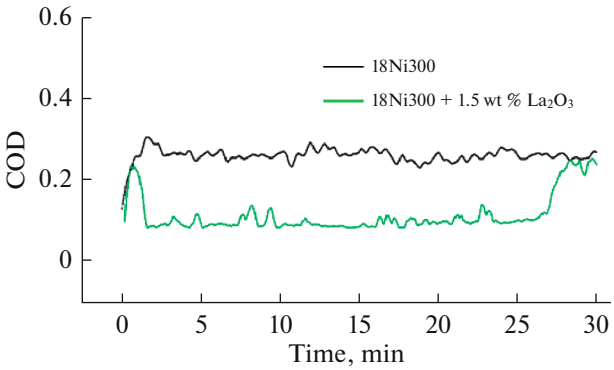

Fig. 10. Friction coefficient of 18Ni300 and 18Ni300 + 1.5 wt % La_2O_3 cladded layers.

amount is 1.5 wt %. However, the thermal shock resistance of the cladded layer is greatly deteriorated and becomes invalid after 8 cycles when the addition amount is too high (X = 2 wt %). Cracks appeared in the 18Ni300 + 2 wt % La_2O_3 cladded layer after 6 cycles and large area cracks appeared after 8 cycles.

Because the linear expansion coefficient of the cladding layer and the matrix is different, the internal stress will be generated in the repeated process of thermal expansion and cold contraction. Meanwhile, the impurities in the cladding layer will act as the crack source. When the internal stress is large enough, the cladding layer will crack and eventually fall off from the matrix. When the addition of La_2O_3 is less than 1.5%, with the increase of La_2O_3 content, the cladding grains become finer and more uniform, and the impurities can be eliminated to a certain extent, which improves the overall toughness of the cladding layer and thus improves the thermal shock life of the cladding layer. When the addition of La_2O_3 is more than 2.0%, a large number of unmelted rare earth oxides are mixed in the cladding layer, which greatly worsens the toughness of the cladding layer and greatly reduces the thermal shock life.

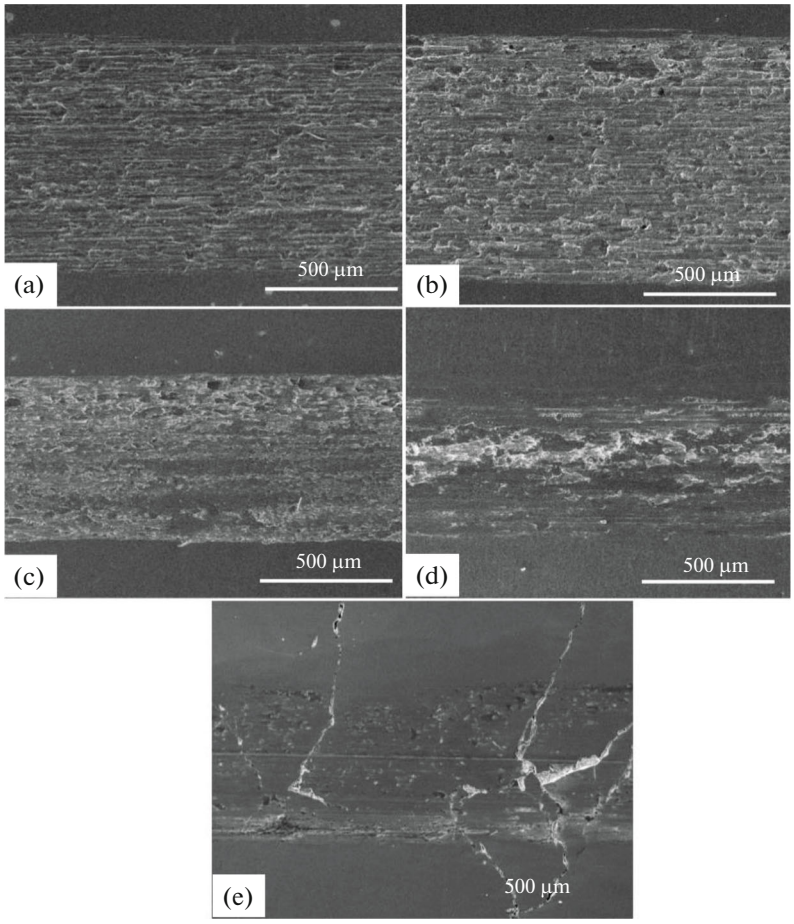

Fig. 11. Wear morphology of the cladded layer 18Ni300 + X wt %La_2O_3: (a) X = 0; (b) X = 0.5 wt %; (c) X = 1 wt %; (d) X = 1.5 wt %; (e) X = 2 wt %.

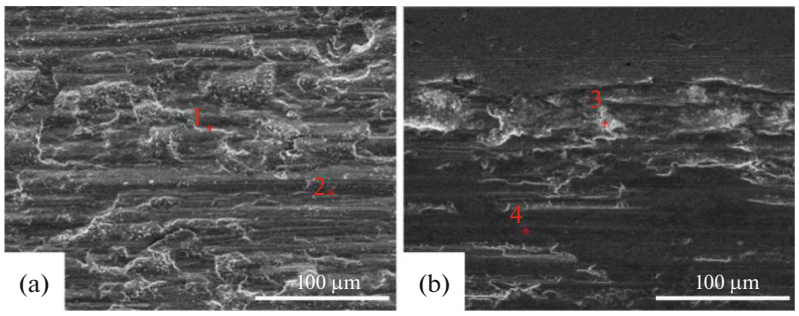

Fig. 12. Comparison of wear morphology of the cladded layer: (a) 18Ni300; (b) 18Ni300 + 1.5 wt % La_2O_3.

4. CONCLUSIONS

In this work, ZL205A aluminum alloy surface is clad with 18Ni300 + La_2O_3 using laser cladding technology. The effect of varying content of La_2O_3 (i.e. 18Ni300 + X La_2O_3 (X (wt %) = 0, 0.5 1.0,1.5 and 2.0) on the microstructure, hardness, wear resistance and heat-thermal shock behavior were investigated. Following are the results that could be drawn from the investigation:

The addition of La_2O_3 (i) eliminated porosity on 18Ni300 cladding surface and leveled the cladding, (ii) refined grains, (iii) inhibited the formation of intermetallic compounds in the fusion zone, (iv) eliminated cracks in the binding zone, and (v) purified the cladding layer microstructure.

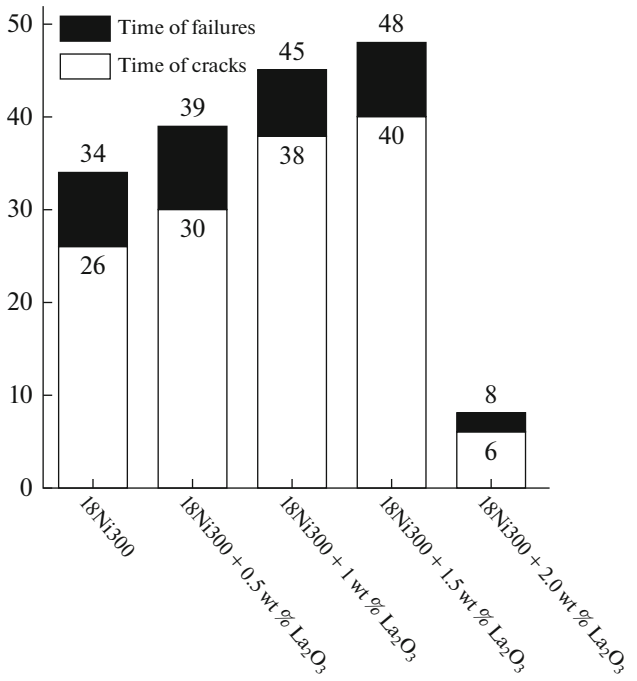

Fig. 13. Thermal shock life of 18Ni300 + X wt % La_2O_3 laser cladded layers.

Grain refinement and purification of the cladding layer organization improved the mechanical properties.

In this study, the optimal content ratio of La_2O_3 added is 1.5 wt %, the hardness is 37 higher than that of 18Ni300, the wear amount is 71% of 18Ni300, and the heat shock resistance is about 41% higher. 18Ni300 + 1.5 wt % La_2O_3 cladding layer showed excellent forming ability, high wear resistance and thermal shock resistance, and is the most suitable material for the inner surface of aluminum alloy laser engine.

FUNDING

This work was sponsored by Key Research and Development Project of Zhejiang Province (2021C04022). Serbia-China Bilateral Science and Technology Cooperation Project no. 17 “Advanced Technologies Based on Pulsed Lasers for Modification/Processing and Synthesis of Selected Metal Materials”. This work was supported by the Institute for Nuclear Research, Russian Academy of Sciences.

CONFLICT OF INTEREST

The authors of this work declare that they have no conflicts of interest.

REFERENCES

1. Wang Lixin and Yuan Feng, China Automobile, No. **003**, 100 (2022).
2. Jia Panjiang and Chen Bangfeng, Light Alloy Process. Technol., No. **11**, 4 (2009).
3. Lu Binghen and Li Dichen, Mach. Build. Autom. **42** (4), 1–4 (2013).
4. Gu Dongdong and Shen Yifu., Manuf. Technol., No. 8, 33 (2012).
5. H. B. Amir, R. Armin, F. M. S. Nor, et al., Mater. Sci. Eng. **754** (29), 728 (2019).
6. Chen Guanxiu, An Lizhou, Wang Shuo, et al., Mech. Electr. Prod. Dev. Innovation **35** (5), 5 (2022).
7. J. Liang, L. Wang, X. Zhang, et al., J. Mater. Process. Technol. **117**, 145 (2021)
8. C. M. Grohol, Y. C. Shin, and A. Frank, Surf. Coat. Technol., 439 (2022).
9. T. Wiegold and S. Klinge, PAMM **20**, 181 (2021). https://doi.org/10.1002/pamm.202000181
10. Han Xiaoying, Li Ping, WangYong, et al., China Nonferrous Met., No. 2, 29 (2010).
11. Zhang Liang, Lin Chen, Liu Jia, et al., Appl. Laser, No. 005, 041 (2021).
12. Sun Junsheng, Xu Hu, Guan Changyong, et al., Aeronaut. Manuf. Technol., **65** (15), 7 (2022).
13. Zhang Guangyao, Wang Chenglei, Gao Yuan, Wei Wenzhu, Lu Xiaohui, Zhang Yan, and Wu Weiqin., Mater. Mech. Eng., **39** (07), 69 (2015).
14. Xie Yingguang, Wang Chenglei, Zhang Kexiang, et al., Surf. Technol., No 012, **049** (2020).
15. Wang Chenglei, Liang Zhaojie, Zhou Chenghua, et al., Surf. Technol. **49** (10), 12 (2020).
16. L. P. Lei, Y. E. Hong, K. Song, et al., Surf. Technol. **540**, 13 (2018).
17. Zhang Kang, Bao Junfeng, and Wang Xingyu, Metall. Mater. **41** (04), 66 (2021).
18. P. Farahmand, S. Liu, Z. Zhang, et al., Ceram. Int. **40** (10), 15421 (2014).
19. M. M. Quazi, M. A. Fazal, and A. S. M. A. Haseeb, J. Rare Earths **34** (06), 549 (2016).
20. S. P. Sharma, D. K. Dwivedi, and P. K. Jain, Wear **267** (5–8), 853 (2009).